Influence of π–π Stacking on the self-assembly and coiling of multi-chromophoric polymers based on perylenebis(dicarboximides): An AFM study

ARTICLE *in* SOFT MATTER · NOVEMBER 2009

Impact Factor: 4.03 · DOI: 10.1039/B912302D · Source: OAI

8 AUTHORS, INCLUDING:

Vincenzo Palermo
Italian National Research Council
130 PUBLICATIONS **2,637** CITATIONS
SEE PROFILE

Andrea Liscio
Italian National Research Council
68 PUBLICATIONS **1,252** CITATIONS
SEE PROFILE

Alan E Rowan
Radboud University Nijmegen
304 PUBLICATIONS **10,217** CITATIONS
SEE PROFILE

Paolo Samorì
University of Strasbourg
276 PUBLICATIONS **7,446** CITATIONS
SEE PROFILE

Influence of π–π stacking on the self-assembly and coiling of multi-chromophoric polymers based on perylenebis(dicarboximides): an AFM study†

Vincenzo Palermo,*[a] Erik Schwartz,[b] Andrea Liscio,[a] Matthijs B. J. Otten,[b] Klaus Müllen,*[c] Roeland J. M. Nolte,[b] Alan E. Rowan*[b] and Paolo Samorì*[ad]

Received 23rd June 2009, Accepted 4th August 2009
First published as an Advance Article on the web 22nd September 2009
DOI: 10.1039/b912302d

The assembly behavior at surfaces of very stiff polyisocyanopeptides (PICs) functionalized with semiconducting perylenebis(dicarboximide) (PDI) side chains has been investigated by atomic force microscopy. These multi-chromophoric arrays are unique as they combine an ultra-stiff central polymer main-chain scaffold upon which the PDI chromophores can self-organize through π–π stacking, making them interesting and versatile building blocks for nanoelectronics. In this paper we compare three PIC derivatives featuring different side groups: **M1**—no chromophores, **M2**—chromophores capable of π–π stacking, and **M3**—chromophores where the stacking is hindered by the presence of bulky substituents in the bay area of the PDI. The effect of the different side functionalizations on the macromolecule assembly at surfaces was compared by studying the morphology and aggregation tendency of all three polymers when adsorbed on silicon, mica and graphite substrates. Making use of nano-manipulation of these functional rods with the AFM tip gave insight into the polymer structure and its coiling behaviour.

Introduction

In the last few years, numerous organic semiconducting materials have been developed as active components of various novel microelectronic devices such as light-emitting diodes,[1–3] transistors,[4–8] foldable displays[9] and solar cells.[10,11] A significant advantage of organic semiconductors over conventional inorganic semiconductors is the solution processability of such materials which makes it possible to deposit molecules on solid substrates using cheap techniques such as dipping, drop-casting or spin-coating. In any deposition from solution, the ultimate film morphology depends on a complex balance between molecule–molecule, molecule–substrate, solvent–molecule and solvent–substrate interactions.[12]

Two classes of molecular systems are commonly used for (opto)electronic applications: long π-conjugated polymers, which are easy to process and typically arrange in good uniform layers, and small aromatic molecules, which can form highly defined (liquid) crystalline arrays. Polymer-based systems typically exhibit a low degree of order at the mesoscopic level because the film formation is usually a kinetically governed process[13] that results in architectures exhibiting a relatively low charge mobility compared to that of more ordered (liquid) crystalline materials. On the other hand, small poly-aromatic molecules interact with each other through weak, reversible supramolecular interactions (van der Waals forces, hydrogen bonds, *etc.*) yielding a self-assembly through primarily a thermodynamically controlled process leading to the formation of highly ordered materials possessing very high charge carrier mobilities.[14] These latter molecular systems are, however, often difficult to process due to their crystalline nature.

Recently, a new class of molecules has been presented which combines the main advantages of both the polymeric and the small self-assembling building blocks.[15,16] The underlying design principle of these molecules is the presence of a highly rigid polymeric scaffold which aligns and orders the functional groups attached in the peripheral positions. The molecules (Scheme 1) consist of five essential parts: (i) a highly rigid and all-carbon poly(isocyanide) backbone which adopts a helical conformation when bulky groups are attached to its backbone;[17,18] (ii) chiral alanine side chains that interact through hydrogen bonding, not only inducing the backbone to adopt a 4_1 (four repeat units per turn) helical conformation with a preferred handedness, but also providing greater rigidity and stability to the polymer;[19] (iii) a small flexible linker that obliges the chromophores to remain close to the polymeric chain but it simultaneously allows them to orientate on a molecular scale to maximize their π–π interactions; (iv) the aromatic chromophore that provides electronic and optical function to the architecture; and finally (v) flexible alkyl side chains, which offer increased solubility in organic solvents. The combination of these parts results in high molecular weight

[a]*Instituto per la Sintesi Organica e la Fotoreattività, Consiglio Nazional delle Ricerche, Via Gobetti 101, I-40129 Bologna, Italy. E-mail: palermo@isof.cnr.it*
[b]*Institute for Molecules and Materials, Radboud University Nijmegen, Heyendaalseweg 135, 6525 AJ Nijmegen, The Netherlands. E-mail: a.rowan@science.ru.nl*
[c]*Max-Planck Institute for Polymer Research, Ackermann 10, 55124 Mainz, Germany. E-mail: muellen@mpip-mainz.mpg.de*
[d]*Nanochemistry Laboratory, ISIS, Université de Strasbourg and CNRS (UMR 7006), 8 allée Gaspard Monge, F-67000 Strasbourg, France. E-mail: samori@isis-ulp.org*

† Electronic supplementary information (ESI) available: AFM Figures S1–S4 and Figure S5, which shows GPC traces of **M2**. See DOI: 10.1039/b912302d

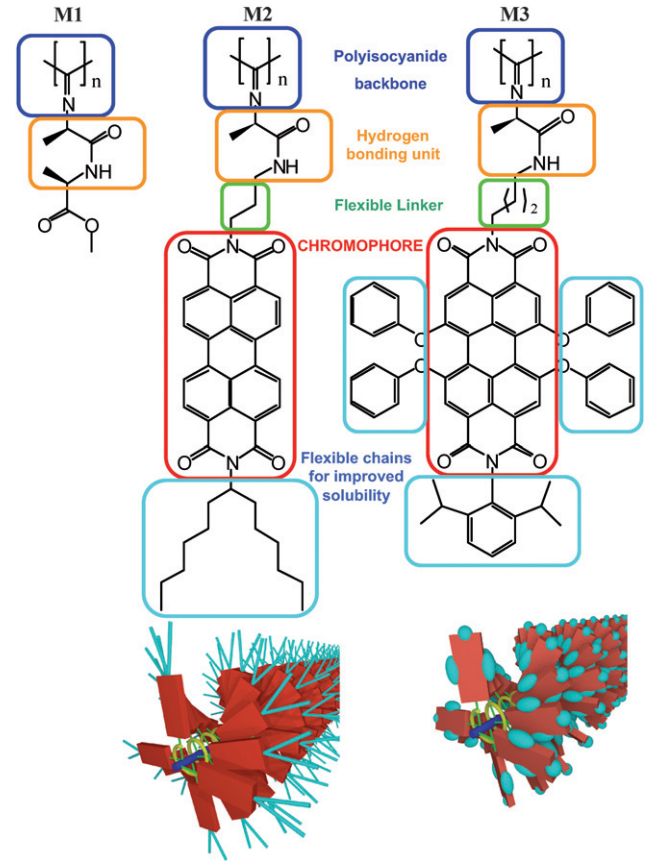

Scheme 1 Structure of the three polymers **M1–M3**. The different moieties constituting the molecule, each one responsible for a specific function, are shown in different colors. A schematic cartoon of the 3-D structure of **M2** and **M3** is also shown. The orientation of the chromophores and side chains with respect to the central backbone is just indicative.

macromolecules possessing extremely high rigidity, good solution processability, and the capacity to generate and transport charges. These molecules have been very recently exploited as active material in transistors[20,21] and solar cells.[22,23]

As aromatic chromophore we have chosen perylenebis(dicarboximides) (PDIs) since they are well-known as organic semiconductors,[24–27] widely used for the fabrication of transistors[28–30] and solar cells.[31–34] Recently several groups have shown that these chromophoric systems feature interesting self-assembly properties. Depending on experimental parameters, such as the type of solvent and the deposition conditions, different interesting morphologies, including polycrystalline layers composed of needle-like crystals having sizes from tens of nm up to a few μm were obtained.[28,35–43]

The synthesis of our complex macromolecules is modular: by changing one among the different moieties, the mechanical, electronic and optical properties of the architectures can be tuned. While extensive characterization of these molecules has already been performed in solution and on macroscopic scale,[15,44,45] it is important to understand how the self-assembly behavior of the side chromophoric groups can be controlled when deposited in thin layers, since this will influence the morphology of the overall macromolecular system and hence the properties of any resulting device.

To address this issue, the present paper offers a comparative study of three different poly(isocyanides), shown in Scheme 1, which can be expected to feature different intra- and intermolecular interactions. Polymer **M1** consists of a central poly(isocyanide) backbone derived from alanine side chains terminating with a methoxy end group. Previous studies revealed that on mica single strands of this macromolecule can be visualized and they were found to possess a persistence length as high as 76 nm, thus greater than that of dsDNA chains.[46] Such an impressive high rigidity is a result of the helical conformation of the polymer which is further stabilized by H-bonding between amide groups in the n and $n + 4$ position, resulting in four β-sheet arrays which run along the polymer backbone. **M2** possesses flat PDI moieties at the end of alanine side chain of **M1** that can interact through π–π stacking, thus forming long PDI stacks running along the polymer chain. **M3** possesses bulky PDIs at the end of the alanine side chain of **M1**, which hinders π–π interactions between the PDIs attached to the polymer backbone. The use of a slightly longer aliphatic spacer bridging the polymer backbone with the PDI provides greater conformational flexibility and hence can overcome (and 'overrule') the steric hindrance brought into play by the presence of the four large phenoxy groups in the bay area of the PDI chromophore.

UV-Vis spectroscopy of **M2**[45] indicates strong interactions between the PDIs attached in position n and $n + 4$ leading to a 4.2 Å stacking distance between two adjacent PDI cores adopting a face-to-face arrangement. The absorption spectrum of **M3** resembles the spectrum of PDI dimers. This could indicate H-aggregation of the PDIs, however, the absence of a red shifted component is atypical and has not been observed in the dimer systems.[47] Besides exciton coupling, changes in the spectrum might also be caused by conformational changes induced by steric interactions between the bulky PDIs, which make the interpretation of the absorption spectra more complex.[45]

To gain a detailed understanding on the assembly behavior of the polymers **M1–M3** on surfaces, the materials were spin-coated onto three different, atomically flat, solid substrates, *viz.* highly oriented pyrolytic graphite, silicon covered with a 2 nm thick native oxide layer and muscovite mica. Whereas graphite is an all-carbon, apolar and electrically conducting crystal, SiO_x features a polar surface, exposing Si–O–Si and Si–O–H moieties. Mica is a poly-electrolyte, and hence a highly polar, substrate. We employed three different substrates in order to gain information about the interfacial interactions, which could lead to particular surface morphologies.

Experimental conditions

The synthesis of the multi-chromophoric arrays has been described elsewhere.[45] The polymers exhibit good solubility in many organic solvents, allowing a detailed characterization by UV-Vis, fluorescence and infrared spectroscopy, as well as circular dichroism.[45]

Sub-monolayer thick films of **M1**, **M2** and **M3** were prepared from solutions in $CHCl_3$ of each molecule (30 mg L^{-1}) spin-coated (2000 rpm) onto graphite, muscovite mica and single crystal silicon (100) substrates. HOPG and mica substrates were cleaved right before spin-coating, whereas silicon was cleaned using a standard RCA procedure,[48] which uses a hydrogen

peroxide solution to remove organic contaminants present on the surface, and leaves it covered with a 1–2 nm thick layer of highly hydrophilic oxide.

The deposited polymeric fibers have been characterized by atomic force microscopy (AFM)[49,50] (Nanoscope III instrument, Digital Instruments). All images were recorded with the AFM operating in tapping-mode in air at room temperature with a resolution of 512 × 512 pixels using moderate scan rates (1–2 lines per second). The polymer chains' dimensions were estimated from topographical profiles and the values obtained were corrected for the tip broadening effect, assuming a tip radius of 13 nm.[51] For the uncoiling experiments the AFM was operated using very small values of amplitude set points, to maximize the tip–substrate interactions. The uncoiling of the molecules using contact mode AFM was also tested, but resulted in damage of the molecules. Commercial tapping-mode tips (RTESP, Veeco) were used with resonance frequencies of ~300 kHz and force constant of ~40 N m^{-1}.

Results

Topographical AFM images on sub-monolayer thick films revealed that both polymers **M1** and **M2** tend to assemble into bundles of fibers on all three substrates, although subtle differences in the fiber's morphology were observed (Fig. 1).

Polymer **M1** was found to form bundles of fibers on all the employed substrates, with a slightly different morphology due to the different substrate roughness and chemical nature. On graphite a great variation of fibers' dimension is found, with bundles' width ranging from 10 to 50 nm. On silicon, the bundles have smaller widths and larger heights, with a more irregular morphology of the fibers. A more defined morphology was found on mica, where fibers' knots and bends can be observed. Widths and heights of single fibers are listed in Tables 1 and 2, respectively.[52]

Polymer **M2** was also found to assemble into bundles of many single polymer strands, indicating a strong tendency to form inter-chain interactions. On graphite, large bundle widths were obtained, due to the supercoiling of polymers (see below), while on silicon a more disordered network was observed. On graphite, for **M2** (and to a lesser extent for **M1**) a large range of heights and widths was observed, and in some areas sharp changes of

Table 1 Width (in nm) of the structures formed on each substrate

	M1	M2	M3
Graphite	33 ± 17	55 ± 20	57 ± 27
Si	26 ± 10	24 ± 11	28 ± 11
Mica	25 ± 10	42 ± 9	22 ± 9

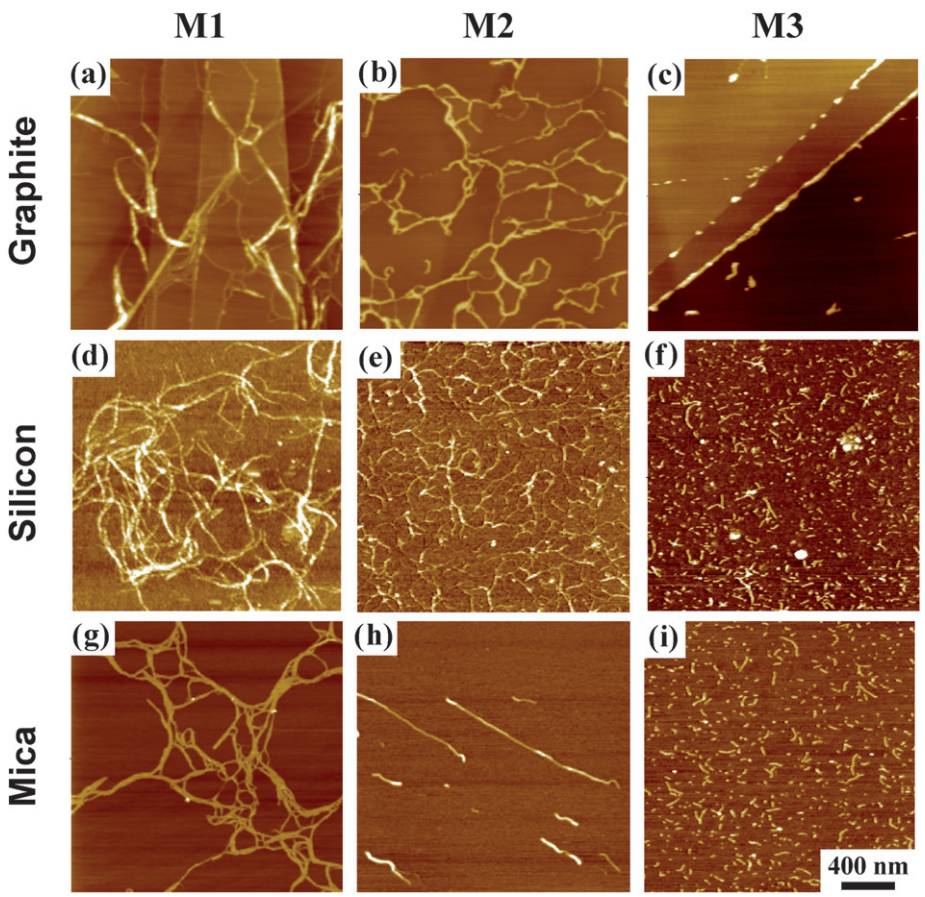

Fig. 1 Unfiltered, AFM height images of the morphologies of ultrathin films of **M1**, **M2** and **M3** on graphite, silicon and mica, respectively. The image width is 2 μm for each frame. *Z*-Ranges are: (a) 10 nm, (b) 10 nm, (c) 5 nm, (d) 10 nm, (e) 5 nm, (f) 5 nm, (g) 5 nm, (h) 5 nm and (i) 5 nm. The same AFM images with a *Z*-range = 10 nm are shown in Fig. S2 in the ESI†.

Table 2 Height (in nm) of the structures formed on each substrate

	M1	M2	M3
Graphite	0.9 ± 0.3	2.2 ± 0.5	3 ± 0.8
Si	2.4 ± 0.8	1.6 ± 0.6	2.4 ± 0.6
Mica	0.8 ± 0.3	1.4 ± 0.8	1.9 ± 0.2

fiber width from 9 ± 6 nm to 12 ± 6 nm were measured, probably as a result of the supercoiling of multiple chains to form bundles (Fig. 2b and c). On mica, interestingly, the bundles of **M2** were found to be aligned in some areas along one direction, on the tens of microns scale, due to the effect of a hydrodynamic flow during spin-coating (Fig. 1h).[53]

Conversely, polymer **M3** shows shorter polymer strands adsorbed on all three substrate surfaces. This can be explained by the slow polymerization of the isocyanide monomer, which is caused by the bulkiness of the PDIs in **M3**. On the mica surface, **M3** reveals short linear segments coexisting with rounded structures. On graphite, the **M3** polymers preferentially adsorb at surface defects, such as the graphite step edges. Alongside the preferential adsorption at the step edges on graphite, the **M3** polymer molecules show a low tendency to aggregate, evidenced by the presence of many isolated molecules randomly distributed on the various substrates. In contrast to the other polymers, the short **M3** macromolecules can in fact seldom be observed to physically interact with one another (see Fig. 2a). This observation could also be the result of the larger steric hindrance of **M3** side substituents, which block π–π stacking of PDIs to a large extent, both belonging to the same and to different adjacent polymer chains. Thus, **M1** and **M2** possess a well-defined architecture which results in long stiff rods, which have a preference to interact both at the intra- and at the inter-molecular level, whilst the sterically hindered **M3** polymers have a lower tendency to interact. The widths of the polymers measured by AFM (Table 1) are much larger than the molecular diameters calculated by modeling, even after being corrected for the effect of tip broadening.[51] Furthermore, the heights observed (Table 2) are much smaller than those calculated,[44] suggesting that on the surfaces the polymers adopt an elliptical cross-section promoted by the strong polymer molecule–substrate interactions and by the conformational flexibility of the aliphatic side groups that can collapse on the surface.[54,55]

Except for the case on silicon surfaces, the heights of the nanostructures increase from **M1** to **M2**, and finally to **M3**. This result nicely reflects the increase in cross-section of the macromolecules as well as the enhancement in shape persistence of the polymers due to the presence of the PDI dye (for **M2**) and the bulky PDI that exposes sterically demanding phenoxy side groups (for **M3**). The superposition of the two **M3** chains observed in this film is accompanied by an increase in the thickness of the fibers in the second layer if compared to those in the first layer, *viz.* from *circa* 1.9 nm to *circa* 4.9 nm (Fig. 2a). The increased thickness of the chain superimposed onto the one adsorbed directly on the surface is due to the fact that it feels a weaker interaction from the surface, and thus it adopts a cross-section that is more circular in shape, and close to the theoretical cross-section (~5.0 nm).[44]

The difference in the height of the single molecules (and bundles thereof) predicted by modeling with that experimentally determined from topographical profiles in AFM images was previously found to be dramatic when measurements of hydrophobic adsorbates supported on hydrophilic substrates were performed in an atmosphere with a high relative humidity.[46] The origin of this discrepancy between measured and calculated width/height can also include the observed indentation of the macromolecule by the probing AFM tip and the adhesion of the AFM tip to the surface.[19,54,56] This can sometimes even lead to contrast inversion (see Fig. S1 in ESI†). Moreover, additional roles can be ascribed to the indentation of the macromolecule by the probing AFM tip[54] and the adhesion of the AFM tip to the surface.[19,56] Therefore, the heights reported in Table 2 must be considered as being just indicative, and useful only for comparing the different samples.

The intra-molecular coiling in **M2** can be explained in view of the high steric hindrance brought into play by the pendant PDIs, which induces a mechanical stress into the polymeric backbone that can be alleviated *via* bending. Self-coiling can be monitored when isolated **M2** molecules are deposited on graphite at low surface coverages (Fig. 2b). In this case, abrupt variations of fiber's widths and heights are observed in the AFM topographical images as shown in Fig. 2b and c. The increase in the cross-section of the fiber can be either due to intra-molecular coiling, with a single polymeric chain coiling on itself, or due to inter-molecular coiling, *i.e.* two different fibers are coiled in a similar way to DNA double strands. The latter case would give many X- or Y-shaped assemblies, featuring two different fibers

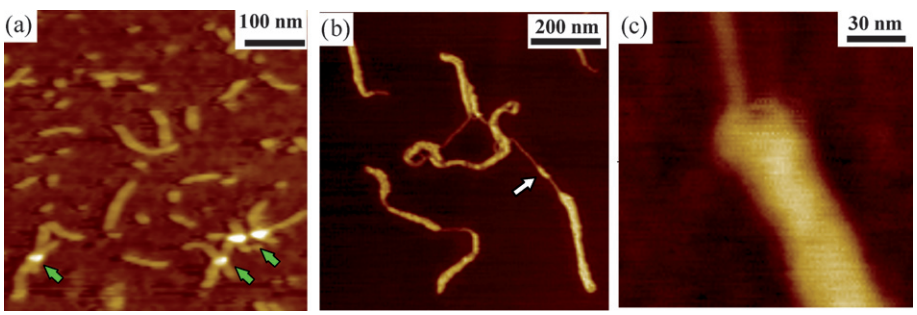

Fig. 2 Unfiltered, AFM height images of (a) **M3** molecules on mica. Arrows show intersecting, superimposed molecules. (b) "Super-coiled" **M2** molecules on graphite and (c) detail of a coiled **M2** fiber. *Z*-Ranges are (a) 7 nm, (b) 5 nm and (c) 5 nm.

that supercoil and then eventually split again. Such assemblies have only been rarely observed on the sample. One could also explain the increase of the fiber's cross-section by assuming that in these areas shorter polymer chains are coiled along the longer one. However, in light of the variable length of the coiled sections, even down to 50 nm (see Fig. 2b, white arrow), one would need the presence of very short and highly polydisperse chains. This case was ruled out by gel permeation chromatography measurements of **M2** (see ESI†, Fig. S5). All this evidence suggests that **M2** molecules can easily undergo intra-molecular coiling when their concentration on the surface is low (see Fig. 2b). Inter-molecular assembly can instead be improved using higher concentrations as can be seen in Fig. 1b, or by using solvent vapor annealing (see below).

To cast more light on the nature of the observed polymer structures, we attempted to stretch them by the application of an external stimulus.[57–59] In Fig. 3, the lateral stretching of **M2** superstructures accomplished with the AFM tip on graphite is displayed. By scanning the surface with low feedback gain and high speed, a change in the molecular shape could be mechanically triggered with the AFM tip: the polymer chains were elongated along the fast scan direction (Fig. 3a). This leads to the generation of an undulated architecture having a very long pitch (up to 150–200 nm), showing sharp bends of ~120°, likely due to the hexagonal symmetry of the mica lattice (Fig. 3b). Such a very long pitch does not reflect the characteristic pitch of the helical individual polymers (see cartoons in Scheme 1), since the latter amounts to one order of magnitude smaller, as obtained from modeling and optical studies.[45] Instead, the observed superstructure is evidence of the molecules' tendency to adopt a coiled conformation. In particular, in Fig. 3c only the central part of a fiber (in between the white arrows) was uncoiled, showing a reduction in height (from ~2 nm to ~1 nm) and a coiled structure. Sharp changes in appearance and width can be observed for fibers which have been only partially uncoiled (Fig. 3c).

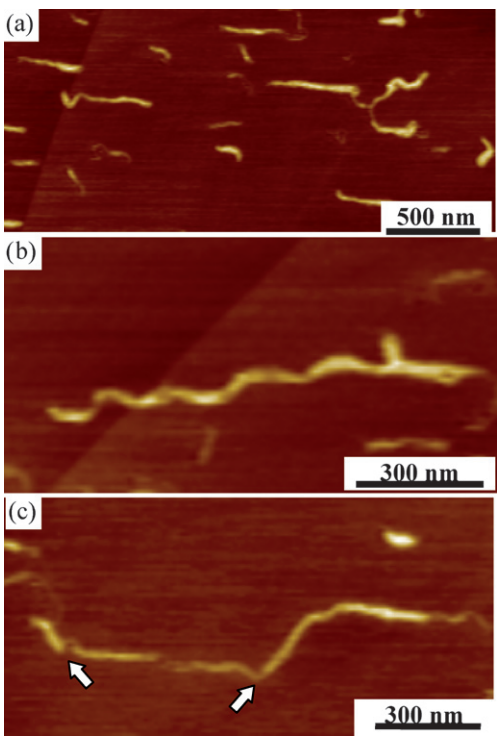

Fig. 3 AFM height images of **M2** fibers uncoiled mechanically using the AFM tip. Fast scan direction of the AFM tip was horizontal in the image. *Z*-Ranges: (a) 5 nm, (b) 5 nm and (c) 5 nm.

Similar mechanical stretching performed on films of **M1** and **M3** did not give any observable uncoiling of the molecules. In **M3** the supercoiling of the molecules is unfavored because of the weaker intra-molecular propensity to aggregate due to the presence of the bulky groups attached to the PDIs, and to the shorter length of the polymers with respect to **M2**. In the case of **M1** the absence of significant intra-molecular supercoiling is likely due to the much weaker aggregation tendency of the methoxy end groups.

By and large, the comparison of the nanoscale morphology of the three polyisocyanide derivatives on the different substrates reveals that, while for **M1** and in particular **M2** strong inter- and intra-molecular interactions are present leading to the formation of bundles and supercoiling, **M3** chains adsorb onto the substrate surface as isolated nano-objects.

Other evidence for the strong tendency of **M2** bundles to interact with each other can be obtained by exposing the samples, after deposition, to solvent vapor annealing.[38,60,61] By exposing a surface to saturated chloroform vapors, a thin layer of liquid condenses on the substrate with a thickness which, depending on experimental conditions, ranges from a few nm to macroscopic droplets.[62] Molecules already deposited on the substrate are partially solubilized by the thin, quasi-2-dimensional solvent layer, acquiring a surface mobility which allows them to rearrange and move on the tens of microns scale.[38] Preliminary experiments have been performed by keeping all the samples of **M1**, **M2** and **M3** shown in Fig. 1 for several days in a closed jar saturated with chloroform vapors. Some rearrangement was observed for all three molecules on all the samples, with only minor changes in the morphology. In the case of **M2** molecules deposited on mica, though, a peculiar result was obtained. Bundles were able to move on the surface and rearrange, interacting with each other. The annealing time was not long enough to completely remove the fibers' alignment; instead, the annealing was stopped while adjacent fiber bundles were blocked in the act of coiling with each other forming Y-shaped bifurcations (arrows in Fig. 4b), a clear evidence of their strong tendency to interact.

Conclusions

The adsorption of three different complex multi-chromophoric arrays on solid substrates has been explored in a comparative study. When the polyisocyanopeptides' central chain is functionalized with side perylenebis(dicarboximide) units that are able to interact with each other by π–π stacking (molecule **M2**), major changes in the polymer structure are observed as compared to molecules where the π–π interaction is not present, either for the lack of the stacking units (**M1**) or for the neutralization of perylene π–π stacking due to steric hindrance (**M3**). When deposited on the substrate, these molecules tend to form well-defined bundles with a strong tendency of the molecules to supercoil. In particular, the major effect of stacking interactions

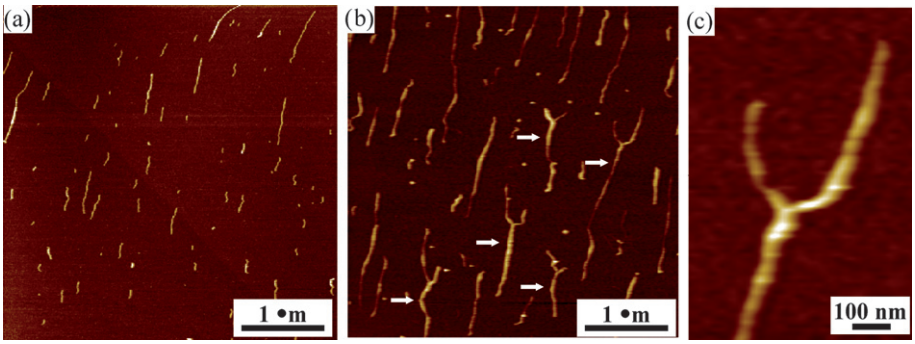

Fig. 4 AFM height images of **M2** on mica before (a) and after (b) solvent vapor annealing. The different densities observed in the images are due to the fact that different areas of the sample were imaged before and after the annealing. Arrows in (b) indicate the Y-shaped intersections caused by the coiling of two **M2** bundles during solvent vapor annealing. (c) Zoom-in of an intersection. *Z*-Ranges: (a) 5 nm, (b) 6 nm and (c) 5 nm.

of the PDI chromophores is to favor both inter-chain and intra-chain interactions, with the molecules tending to form well-defined bundles and supercoils.

The results obtained indicate that, in multi-chromophoric polymers, the relationship between the central PIC backbone and the side functionalizations is not a simple "master–slave" interaction, in which the central backbone dictates the overall morphology and the pending perylene units arrange consequently, only influencing the electronic properties of the material. Instead, the presence of side perylenes has a fundamental role in the material morphology, distinguishing significantly the self-assembling behavior of **M2** from the one of **M1**. This difference is not only due to the steric hindrance of the PDIs, but a fundamental role is also played by their ability to interact with each other, through π–π interactions, as demonstrated by comparing the behavior of **M2** and **M3** molecules.

The overall macromolecular scaffolding approach based on attaching single chromophores to a rigid polymeric chain to study their properties and interactions in a situation of reduced degrees of freedom can be applied to the study of very different kinds of small chromophores, exploring the possibilities offered by the competition between the intrinsic rigidity of the PIC backbone and the self-assembly properties of different side chromophores. This approach may lead to the fabrication of innovative materials for organic electronics where the self-assembling properties and the electronic properties can be tuned independently by changing the nature of the central polymeric backbone and of the side chromophores.

Acknowledgements

We thank B. Simons for help with the AFM measurements. This work was supported by the ESF-SONS2-SUPRAMATES and ESF-SONS-BIONICS projects, as well as the EC-FP7 large scale project ONE-P (no. 212311) and the NanoSciEra project SENSORS.

References

1 R. H. Friend, R. W. Gymer, A. B. Holmes, J. H. Burroughes, R. N. Marks, C. Taliani, D. D. C. Bradley, D. A. Dos Santos, J. L. Brédas, M. Logdlund and W. R. Salaneck, *Nature*, 1999, **397**, 121–128.
2 S. R. Forrest, *Nature*, 2004, **428**, 911–918.
3 F. Cacialli, J. S. Wilson, J. J. Michels, C. Daniel, C. Silva, R. H. Friend, N. Severin, P. Samorì, J. P. Rabe, M. J. O'Connell, P. N. Taylor and H. L. Anderson, *Nat. Mater.*, 2002, **1**, 160–164.
4 H. Sirringhaus, P. J. Brown, R. H. Friend, M. M. Nielsen, K. Bechgaard, B. M. W. Langeveld-Voss, A. J. H. Spiering, R. A. J. Janssen, E. W. Meijer, P. Herwig and D. M. de Leeuw, *Nature*, 1999, **401**, 685–688.
5 L. L. Chua, J. Zaumseil, J. F. Chang, E. C. W. Ou, P. K. H. Ho, H. Sirringhaus and R. H. Friend, *Nature*, 2005, **434**, 194–199.
6 M. Muccini, *Nat. Mater.*, 2006, **5**, 605–613.
7 J. Cornil, J. L. Brédas, J. Zaumseil and H. Sirringhaus, *Adv. Mater.*, 2007, **19**, 1791–1799.
8 A. Facchetti, *Mater. Today (Oxford, UK)*, 2007, **10**, 28–37.
9 J. Jang, *Mater. Today (Oxford, UK)*, 2006, **9**, 46–52.
10 J. J. M. Halls, C. A. Walsh, N. C. Greenham, E. A. Marseglia, R. H. Friend, S. C. Moratti and A. B. Holmes, *Nature*, 1995, **376**, 498–500.
11 G. Yu, J. Gao, J. C. Hummelen, F. Wudl and A. J. Heeger, *Science*, 1995, **270**, 1789–1791.
12 V. Palermo and P. Samorì, *Angew. Chem., Int. Ed.*, 2007, **46**, 4428–4432.
13 P. Müller-Buschbaum, *J. Phys.: Condens. Matter*, 2003, **15**, R1549–R1582.
14 V. C. Sundar, J. Zaumseil, V. Podzorov, E. Menard, R. L. Willett, T. Someya, M. E. Gershenson and J. A. Rogers, *Science*, 2004, **303**, 1644–1646.
15 J. Hernando, P. A. J. de Witte, E. van Dijk, J. Korterik, R. J. M. Nolte, A. E. Rowan, M. F. Garcia-Parajo and N. F. van Hulst, *Angew. Chem., Int. Ed.*, 2004, **43**, 4045–4049.
16 P. A. J. de Witte, M. Castriciano, J. Cornelissen, L. M. Scolaro, R. J. M. Nolte and A. E. Rowan, *Chem.–Eur. J.*, 2003, **9**, 1775–1781.
17 J. J. L. M. Cornelissen, J. J. J. M. Donners, R. de Gelder, W. S. Graswinckel, G. A. Metselaar, A. E. Rowan, N. A. J. M. Sommerdijk and R. J. M. Nolte, *Science*, 2001, **293**, 676–680.
18 J. J. L. M. Cornelissen, A. E. Rowan, R. J. M. Nolte and N. A. J. M. Sommerdijk, *Chem. Rev.*, 2001, **101**, 4039–4070.
19 P. Samorì, C. Ecker, I. Goessl, P. A. J. de Witte, J. J. L. M. Cornelissen, G. A. Metselaar, M. B. J. Otten, A. E. Rowan, R. J. M. Nolte and J. P. Rabe, *Macromolecules*, 2002, **35**, 5290–5294.
20 C. E. Finlayson, R. H. Friend, M. B. J. Otten, E. Schwartz, R. J. M. Nolte, A. E. Rowan, V. Palermo, A. Liscio, P. Samorì, K. Paneva, K. Müllen, S. Trapani and D. Beljonne, *Adv. Funct. Mater.*, 2008, **18**, 3947.
21 R. Dabirian, V. Palermo, A. Liscio, E. Schwartz, M. B. J. Otten, C. E. Finlayson, E. Treossi, R. H. Friend, G. Calestani, K. Müllen, R. J. M. Nolte, A. E. Rowan and P. Samorì, *J. Am. Chem. Soc.*, 2009, **131**, 7055–7063.
22 V. Palermo, M. B. J. Otten, A. Liscio, E. Schwartz, P. A. J. de Witte, M. A. Castriciano, M. M. Wienk, F. Nolde, G. De Luca, J. J. L. M. Cornelissen, R. A. J. Janssen, K. Müllen, A. E. Rowan, R. J. M. Nolte and P. Samorì, *J. Am. Chem. Soc.*, 2008, **130**, 14605–14614.
23 S. Foster, C. E. Finlayson, P. E. Keivanidis, Y.-S. Huang, I. Hwang, M. B. J. Otten, L. L. Lu, E. Schwartz, R. J. M. Nolte and A. E. Rowan, *Macromolecules*, 2009, **42**, 2023–2030.

24 C. W. Struijk, A. B. Sieval, J. E. J. Dakhorst, M. van Dijk, P. Kimkes, R. B. M. Koehorst, H. Donker, T. J. Schaafsma, S. J. Picken, A. M. van de Craats, J. M. Warman, H. Zuilhof and E. J. R. Sudholter, *J. Am. Chem. Soc.*, 2000, **122**, 11057–11066.
25 F. Würthner, *Chem. Commun.*, 2004, 1564–1579.
26 J. Elemans, R. Van Hameren, R. J. M. Nolte and A. E. Rowan, *Adv. Mater.*, 2006, **18**, 1251–1266.
27 F. Nolde, W. Pisula, S. Muller, C. Kohl and K. Müllen, *Chem. Mater.*, 2006, **18**, 3715–3725.
28 A. L. Briseno, S. C. B. Mannsfeld, C. Reese, J. M. Hancock, Y. Xiong, S. A. Jenekhe, Z. Bao and Y. Xia, *Nano Lett.*, 2007, **7**, 2847–2853.
29 Y. K. Che, A. Datar, K. Balakrishnan and L. Zang, *J. Am. Chem. Soc.*, 2007, **129**, 7234–7235.
30 H. N. Tsao, W. Pisula, Z. H. Liu, W. Osikowicz, W. R. Salaneck and K. Müllen, *Adv. Mater.*, 2008, **20**, 2715–2719.
31 J. J. Dittmer, R. Lazzaroni, P. Leclère, P. Moretti, M. Granstrom, K. Petritsch, E. A. Marseglia, R. H. Friend, J. L. Brédas, H. Rost and A. B. Holmes, *Sol. Energy Mater. Sol. Cells*, 2000, **61**, 53–61.
32 J. L. Li, F. Dierschke, J. S. Wu, A. C. Grimsdale and K. Müllen, *J. Mater. Chem.*, 2006, **16**, 96–100.
33 L. Schmidt-Mende, A. Fechtenkötter, K. Müllen, E. Moons, R. H. Friend and J. D. MacKenzie, *Science*, 2001, **293**, 1119–1122.
34 W. S. Shin, H. H. Jeong, M. K. Kim, S. H. Jin, M. R. Kim, J. K. Lee, J. W. Lee and Y. S. Gal, *J. Mater. Chem.*, 2006, **16**, 384–390.
35 K. Balakrishnan, A. Datar, R. Oitker, H. Chen, J. M. Zuo and L. Zang, *J. Am. Chem. Soc.*, 2005, **127**, 10496–10497.
36 K. Balakrishnan, A. Datar, T. Naddo, J. L. Huang, R. Oitker, M. Yen, J. C. Zhao and L. Zang, *J. Am. Chem. Soc.*, 2006, **128**, 7390–7398.
37 V. Palermo, A. Liscio, D. Gentilini, F. Nolde, K. Müllen and P. Samorì, *Small*, 2006, **3**, 161–167.
38 G. De Luca, A. Liscio, P. Maccagnani, F. Nolde, V. Palermo, K. Müllen and P. Samorì, *Adv. Funct. Mater.*, 2007, **17**, 3791–3798.
39 W. Su, Y. X. Zhang, C. T. Zhao, X. Y. Li and J. Z. Jiang, *ChemPhysChem*, 2007, **8**, 1857–1862.
40 Z. J. Chen, V. Stepanenko, V. Dehm, P. Prins, L. D. A. Siebbeles, J. Seibt, P. Marquetand, V. Engel and F. Würthner, *Chem.–Eur. J.*, 2007, **13**, 436–449.
41 J. Q. Feng, B. L. Liang, D. L. Wang, H. X. Wu, L. Xue and X. Y. Li, *Langmuir*, 2008, **24**, 11209–11215.
42 T. E. Kaiser, V. Stepanenko and F. Würthner, *J. Am. Chem. Soc.*, 2009, **131**, 6719–6732.
43 R. Schmidt, J. H. Oh, Y. S. Sun, M. Deppisch, A. M. Krause, K. Radacki, H. Braunschweig, M. Konemann, P. Erk, Z. A. Bao and F. Würthner, *J. Am. Chem. Soc.*, 2009, **131**, 6215–6228.
44 P. A. J. de Witte, J. Hernando, E. E. Neuteboom, E. M. H. P. van Dijk, S. C. J. Meskers, R. A. J. Janssen, N. F. van Hulst, R. J. M. Nolte, M. F. Garcia-Parajo and A. E. Rowan, *J. Phys. Chem. B*, 2006, **110**, 7803–7812.
45 E. Schwartz, V. Palermo, C. E. Finlayson, Y.-S. Huang, M. B. J. Otten, A. Liscio, S. Trapani, I. González-Valls, P. Brocorens, J. J. L. M. Cornelissen, K. Paneva, K. Müllen, F. Spano, R. H. Friend, D. Beljonne, R. J. M. Nolte, P. Samorì and A. E. Rowan, *Chem.–Eur. J.*, 2009, **15**, 2536–2547.
46 W. Zhuang, C. Ecker, G. A. Metselaar, A. E. Rowan, R. J. M. Nolte, P. Samorì and J. P. Rabe, *Macromolecules*, 2005, **38**, 473–480.
47 T. van der Boom, R. T. Hayes, Y. Y. Zhao, P. J. Bushard, E. A. Weiss and M. R. Wasielewski, *J. Am. Chem. Soc.*, 2002, **124**, 9582–9590.
48 W. Kern and D. A. Puotinen, *RCA Rev.*, 1970, **31**, 187–206.
49 P. Samorì, M. Surin, V. Palermo, R. Lazzaroni and P. Leclère, *Phys. Chem. Chem. Phys.*, 2006, **8**, 3927–3938.
50 P. Samorì, *Chem. Soc. Rev.*, 2005, **34**, 551–561.
51 P. Samorì, V. Francke, T. Mangel, K. Müllen and J. P. Rabe, *Opt. Mater. (Amsterdam)*, 1998, **9**, 390–393.
52 Because, in most samples, large aggregates of bundles of different dimensions were observed, the reported heights and widths were measured on the smaller fibers found on the substrate.
53 M. B. J. Otten, C. Ecker, G. A. Metselaar, A. E. Rowan, R. J. M. Nolte, P. Samorì and J. P. Rabe, *ChemPhysChem*, 2004, **5**, 128–130.
54 S. A. Prokhorova, S. S. Sheiko, M. Moller, C. H. Ahn and V. Percec, *Macromol. Rapid Commun.*, 1998, **19**, 359–366.
55 J. Tang, J. W. Li, C. Wang and C. L. Bai, *J. Vac. Sci. Technol., B*, 2000, **18**, 1858–1860.
56 S. J. T. Van Noort, K. O. Van der Werf, B. G. De Grooth, N. F. Van Hulst and J. Greve, *Ultramicroscopy*, 1997, **69**, 117–127.
57 A. F. Zhang, J. Barner, I. Goessl, J. P. Rabe and A. D. Schlüter, *Angew. Chem., Int. Ed.*, 2004, **43**, 5185–5188.
58 P. Samorì, *J. Mater. Chem.*, 2004, **14**, 1353–1366.
59 R. Al-Hellani, J. Barner, J. P. Rabe and A. D. Schlüter, *Chem.–Eur. J.*, 2006, **12**, 6542–6551.
60 G. De Luca, A. Liscio, F. Nolde, L. M. Scolaro, V. Palermo, K. Müllen and P. Samorì, *Soft Matter*, 2008, **4**, 2064–2070.
61 E. Treossi, A. Liscio, X. L. Feng, V. Palermo, K. Müllen and P. Samorì, *Small*, 2009, **5**, 112–119.
62 P. G. De Gennes, *Rev. Mod. Phys.*, 1985, **57**, 827–863.

